This is an open access article published under a Creative Commons Non-Commercial No Derivative Works (CC-BY-NC-ND) Attribution License, which permits copying and redistribution of the article, and creation of adaptations, all for non-commercial purposes.

NANO LETTERS

pubs.acs.org/NanoLett

Letter

Wafer-Scale Growth of One-Dimensional Transition-Metal Telluride Nanowires

Hong En Lim,* Yusuke Nakanishi, Zheng Liu, Jiang Pu, Mina Maruyama, Takahiko Endo, Chisato Ando, Hiroshi Shimizu, Kazuhiro Yanagi, Susumu Okada, Taishi Takenobu, and Yasumitsu Miyata*

Cite This: *Nano Lett.* 2021, 21, 243−249

Read Online

ACCESS | Metrics & More | Article Recommendations | Supporting Information

ABSTRACT: The development of bulk synthetic processes to prepare functional nanomaterials is crucial to achieve progress in fundamental and applied science. Transition-metal chalcogenide (TMC) nanowires, which are one-dimensional (1D) structures having three-atom diameters and van der Waals surfaces, have been reported to possess a 1D metallic nature with great potential in electronics and energy devices. However, their mass production remains challenging. Here, a wafer-scale synthesis of highly crystalline transition-metal telluride nanowires is demonstrated by chemical vapor deposition. The present technique enables formation of either aligned, atomically thin two-dimensional (2D) sheets or random networks of three-dimensional (3D) bundles, both composed of individual nanowires. These nanowires exhibit an anisotropic 1D optical response and superior conducting properties. The findings not only shed light on the controlled and large-scale synthesis of conductive thin films but also provide a platform for the study on physics and device applications of nanowire-based 2D and 3D crystals.

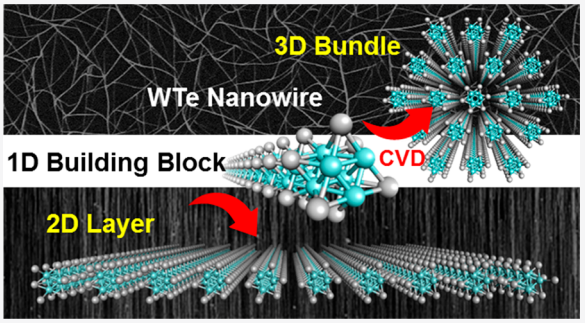

KEYWORDS: *CVD growth, transition-metal chalcogenides, nanowires, 1D building blocks, van der Waals materials*

INTRODUCTION

In recent decades, intensive research has focused on various functional nanomaterials, such as fullerenes,[1] carbon nanotubes (CNTs),[2] graphene,[3] and transition-metal dichalcogenides (TMDCs),[4] because of their excellent physical properties and their wide variety of potential applications such as in electronics and energy conversion devices. The ability to achieve their large-scale synthesis has been key to major breakthroughs that accelerate basic and industrial research. While significant progress has already been made, the synthesis of one-dimensional (1D) transition-metal chalcogenides (TMCs) remains challenging despite 40 years since their discovery in bulk crystals of ternary molybdenum chalcogenides[5−7] and their fascinating physical properties derived from three-atom-thick, 1D quantum confinement system.

A TMC nanowire is a 1D structure consisting of staggered triangular units of M_3X_3, where M = Mo or W and X = S, Se, or Te. Chalcogen atoms occupy the three vertices in each layer and metal atoms are located at the edge centers, resulting in an elongated chalcogen shell with a metal core (Figure 1a). Instead of behaving as a conventional Fermi liquid, such nanowires show 1D metallic behavior consistent with a Tomonaga−Luttinger liquid,[8−10] therefore holding great potential for study in basic physics and electronics applications. In addition, the formation of nanostructures with various geometries is possible due to van der Waals (vdW) interactions between nanowire surfaces. For instance, lateral assembly of these nanowires results in an atomically thin two-dimensional (2D) layer. This may lead to the emergence of interesting physical properties as observed in the semiconducting to metallic transition,[11] large-scale integration of hybrid heterostructures,[12] and anomalous PL properties[13] of ultrathin 2D materials. Besides this, TMC nanowires can also aggregate into three-dimensional (3D) bundles as in the case of CNTs. The 1D confinement effect and structural diversity of TMC nanowires provide an excellent opportunity for further study, as the degree of freedom available during assembly marks an important distinction from other functional nanomaterials.

Despite their attractive features, studies on TMC nanowires are fairly scarce due solely to limited sample availability. A major issue is the lack of a feasible strategy to produce high-quality, long-length nanowires in high yield. Currently available syntheses involve conversion of similar compounds using lithium-intercalated TMC complexes[8,9] or 2H-TMDCs.[10,14,15] A few studies have reported growth using vapor-phase

Received: September 5, 2020
Revised: November 20, 2020
Published: December 14, 2020

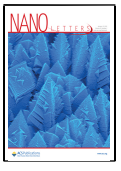

Downloaded via UNIV OF TSUKUBA on April 26, 2022 at 03:10:36 (UTC).
See https://pubs.acs.org/sharingguidelines for options on how to legitimately share published articles.

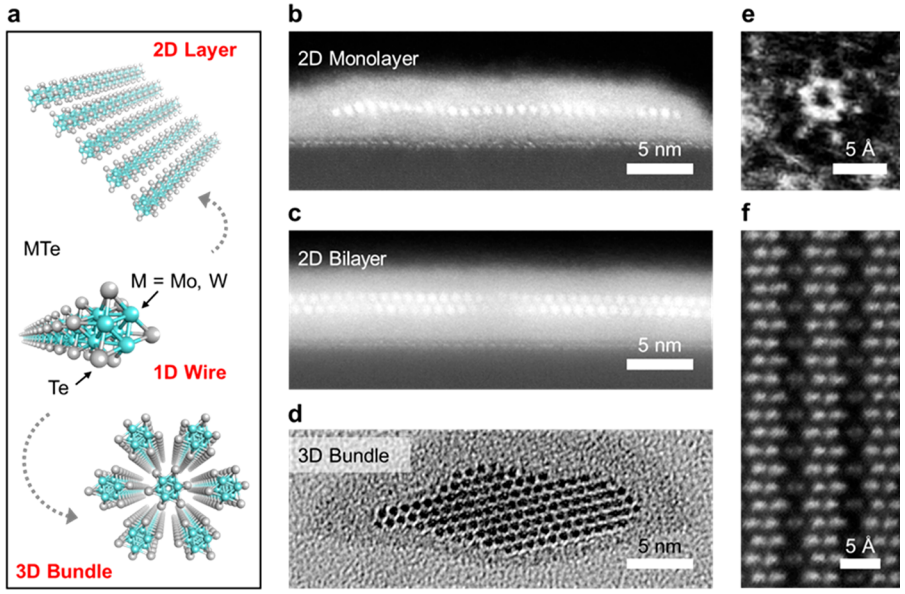

Figure 1. 1D vdW building block. (a) Schematic diagram showing 2D and 3D assemblies of TMC nanowires having the composition *M*Te, where *M* = Mo or W. Each individual wire comprises an elongated network of staggered M_3Te_3 triangular units. Adjacent nanowires interact via vdW forces and either extend laterally, forming a 2D layer, or combine into 3D bundles of various size. (b, c) Cross-section HAADF-STEM images of monolayer and bilayer sheets of WTe nanowires grown on *a*-plane sapphire substrates. (d) Cross-section TEM image of a single WTe 3D bundle grown on a SiO_2/Si substrate. (e) HAADF-STEM image showing the cross-section of a single WTe nanowire. The W core of heavier atomic mass is clearly seen as a bright hexagonal ring surrounded by Te atoms. (f) Atomic resolution HAADF-STEM image of suspended WTe nanowires, illustrating atomic alignment along the nanowire axis.

techniques, such as sulfurization,[16] molecular beam epitaxy,[17] and nanotemplating reaction inside CNTs.[18,19] Although they are reliable fabrication techniques, the mass production and study of TMC nanowires are still constrained by production costs, purity, and scalability.

To solve this issue, we focus our attention on chemical vapor deposition (CVD), which is a powerful technique for the large-scale synthesis of a diverse range of nanomaterials, including CNTs,[20,21] graphene,[22−24] and TMDCs.[25−32] Here, we show wafer-scale growth of WTe and MoTe TMC nanowires, having various aggregation forms, by CVD. The growth substrate is observed to influence the structure and morphology of the TMC nanowires, with random or ordered networks forming on substrates of varying crystallinity and lattice orientation. The present synthesis method enables study of the optical and electronic properties of these TMC nanowire networks, which can be used to benefit future applications in electronics and energy-harvesting devices.

RESULTS AND DISCUSSION

First, 2D and 3D structures based on TMC nanowires, which act as 1D vdW building blocks, are demonstrated by changing growth substrates. Figure 1a shows schematic representations of the different configurations of the TMC nanowires synthesized in this work. Two types of geometrical structures are prepared, with 1D nanowire building blocks forming either an atomically thin 2D sheet or assembling into a 3D bundle. These two structures are observed in the cross-sectional high-angle annular dark-field scanning transmission electron microscopy (HAADF-STEM) and TEM images of the WTe nanowires, as shown in Figure 1b−d. Monolayer and bilayer sheets of WTe nanowires grown on *a*-plane sapphire substrates are presented in Figure 1b and c, respectively, whereas a 3D bundle containing approximately 120 nanowires grown on a SiO_2/Si substrate is displayed in Figure 1d. The atomic structure of the nanowires can be clearly seen from the cross-section image of a single nanowire (Figure 1e) and from the image taken along the nanowire axis (Figure 1f), consistent with those reported for WTe[19] and other TMC nanowires.[14,15,18] The brighter spots in Figure 1e correspond to the heavier atomic mass W atoms. These atoms form a hexagonal ring surrounded by Te atoms having relatively low contrast. Elemental mapping performed by energy dispersive X-ray spectroscopy (EDS) further confirms the chemical composition of the sample (Figures S1 and S2). Quantitative analysis reveals a 1:1 ratio of W to Te, providing further evidence for the identity of the nanowires. Meanwhile, the WTe nanowires in Figure 1b−d are coated with an amorphous layer consisting of W and Te (Figure S3). This amorphous layer is likely residue from decomposed WTe nanowires, caused by damage incurred either by prolonged exposure to the ambient air or during the specimen preparation process.

In addition to the 2D and 3D aggregation forms, the CVD process results in the substrate-dependent formation of aligned and randomly oriented TMC nanowires at the wafer scale. Figure 2a displays the in-house CVD setup used in this study. A temperature range of 750−800 °C was suitable for nanowire growth on various substrates, including SiO_2/Si, quartz, and sapphire. In a typical growth process, precursors such as WO_3 powder and Te granular are heated separately by two furnaces. The alkali metal halide KBr, commonly used in the fabrication of TMDC atomic layers, is also added as a growth promoter near the WO_3. Figure 2b (S4a) and c (S4b) show the as-grown WTe nanowires on SiO_2/Si and sapphire substrates, respectively. In both cases, fiber-like structures are observed to form at high density. A wide coverage of the WTe network is found spanning over a 25 mm × 30 mm growth substrate with uniform sample quality by scanning electron microscopy (SEM) observations and Raman measurements (Figure S5).

https://dx.doi.org/10.1021/acs.nanolett.0c03456
Nano Lett. 2021, 21, 243−249

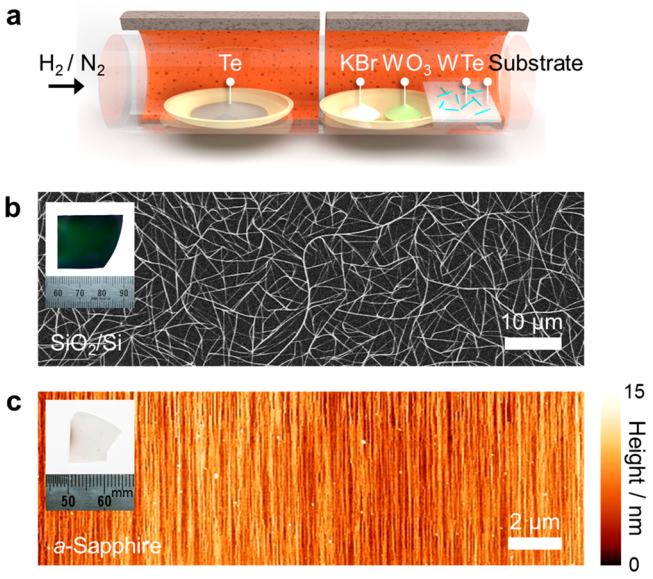

Figure 2. Wafer-scale CVD growth of WTe nanowires. (a) Schematic illustration of the setup used for nanowire synthesis. Growth is conducted via vapor-phase evaporation of solid precursors with the aid of an alkali metal salt as a growth promoter. (b) Plan-view SEM image of the unoriented WTe nanowire arrays grown on a SiO_2/Si substrate. (c) Atomic force microscopy (AFM) topographic image of a dense, ordered array of WTe nanowires synthesized on an *a*-plane sapphire substrate. The insets show the photographic images of the substrate following nanowire growth, which exhibit a slight yellowish (in b) or brownness (in c). The substrate dimensions are approximately 2.5 cm × 3 and 1 cm × 1 cm for (b) and (c), respectively.

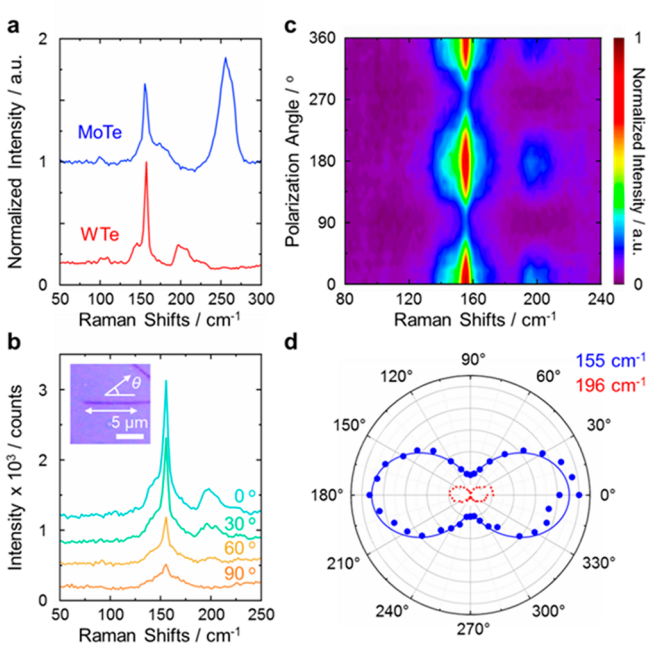

Figure 3. 1D optical response. (a) Normalized Raman spectra for the synthesized MoTe and WTe nanowires on SiO_2/Si. (b) Raman spectra for a single WTe 3D bundle recorded at four representative polarization angles of 0°, 30°, 60°, and 90°. The inset shows an optical image of the sample measured. Theta (θ) refers to the angle between the polarization of the incident laser and the nanowire axis. The spectra in (a) and (b) are shifted vertically for comparison. (c) Polarization-dependent normalized Raman intensity map for corresponding spectra in (b) taken from 0° to 360°. (d) Normalized Raman intensity polar plots for WTe nanowires in (b) at 155 cm^{-1} (blue) and 196 cm^{-1} (red). The solid line is provided as a guide to the eye. Normalization was performed with respect to the peak at 155 cm^{-1} in (a) and the same peak of highest intensity within the range of 0° to 360° in (c) and (d).

While a random network is formed on the silicon substrate in Figure 2b, the use of *a*-plane sapphire results in the growth of aligned fiber-like structures (Figure 2c). The individual aligned fibers have different sizes (Figure S6), with thicknesses ranging from ∼1 to 8 nm. The result agrees with those observed in Figure 1b and c. The growth method described here can also be extended to MoTe (Figure S7). These results clearly indicate that the morphology and growth orientation of TMC nanowires originate from a strong vdW interaction between the TMC nanowires and the substrate. Similar strong substrate interaction has been also observed for the MoS_2 growth on Si(001) surfaces.[13]

The atomically narrow 1D structure of TMC nanowires allows us to probe their 1D optical response. Raman spectra for WTe and MoTe nanowires grown on SiO_2/Si are shown in Figure 3a. Distinct Raman peaks are observed in the range of 50 cm^{-1} to 300 cm^{-1} for both the MoTe and WTe nanowires. Prominent peaks are observed in the vicinity of 155 and 255 cm^{-1} for MoTe, which is similar to that reported previously[17−19] and confirms the identity of the nanowire structure. The former peak is attributed to the out-of-plane stretching of Te atoms, whereas the latter is due to the radial breathing mode of the Mo core.[18,19] This analysis hints at the origins of similar spectral features observed in the WTe sample. Further research into the detailed vibration modes for WTe is currently in progress.

TMC nanowires are expected to display optical anisotropy, as has been observed in many other 1D materials.[24,33−38] We therefore performed polarized Raman spectroscopy measurements on the WTe nanowires grown on a SiO_2/Si substrate. Figure 3b shows the representative Raman spectra measured as the incident angle between the polarized laser and the nanowire axis was varied from 0° to 90°. The Raman signal reaches a maximum when the incident polarized light is parallel to the nanowire axis at 0°. As the incident angle changes, the peaks gradually diminish, reaching a minimum at 90°. Similar results are obtained when the scattered light is collected in parallel or cross configuration relative to the incident laser (Figure S8). Figure 3c presents the polarization-dependent normalized Raman intensity map in the range of 0° to 360°. A uniform optical response is observed for all the different Raman modes, where maximum intensities are observed when the incident polarized beam is parallel to the nanowire axis, at 0°, 180°, and 360°. This gives rise to the 2-fold symmetric polar curves in Figure 3d, where the angular dependences are plotted for the peak intensities at 155 and 196 cm^{-1}.

The above phenomena are similar to those observed in CNTs,[33,34] graphene nanoribbons,[24,35] and semiconducting nanowires such as GaP and InAs[36,37] having anisotropic shapes. For these structures, photon absorption is considerably enhanced when the incident light is polarized parallel to the material's axis. In contrast, excitation using perpendicularly polarized light could be suppressed by the depolarization effect, reducing Raman intensity.[33] The WTe 3D bundles can be conceptually visualized as a structural analogue to bundled CNTs. It is thus expected to exhibit a similar optical response,

https://dx.doi.org/10.1021/acs.nanolett.0c03456
Nano Lett. 2021, 21, 243−249

where a strong depolarization effect is observed, suggesting the 1D nature of the TMC nanowires. Furthermore, the WTe nanowires show three main absorption bands in the visible region at 1.61, 2.34, and 3.02 eV (Figure S9). These absorption bands could account for the polarization-dependent Raman scattering observed through the resonance Raman effect. It should be noted that the phonon confinement effect could lead to the broadening of Raman peaks of WTe bundles as observed for MoS_2 nanoribbons.[38]

In addition to the 1D optical response of the single WTe 3D bundle, the present wafer-scale network of TMC nanowires also shows superior conducting properties. First, the electrical conductivity of a single WTe 3D bundle was monitored using a four-terminal measurement device. As shown in Figure 4a, the

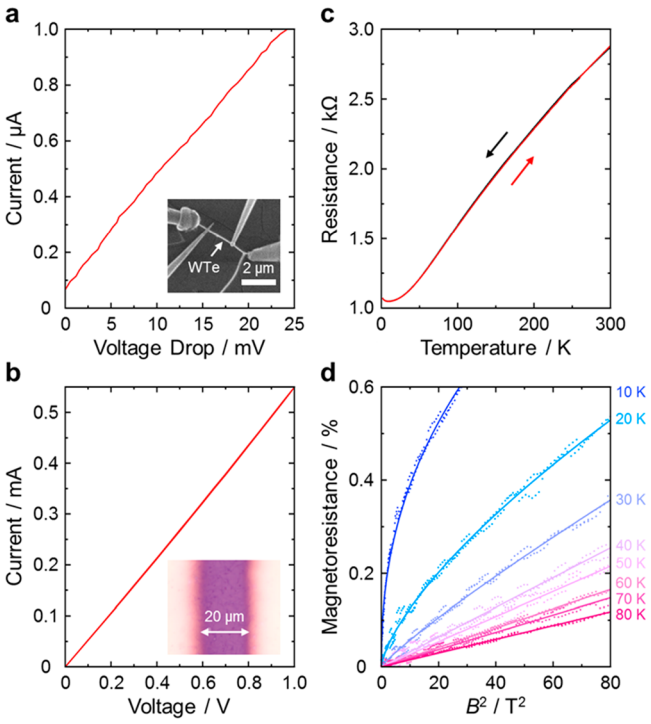

Figure 4. Electron transport properties. $I-V$ characteristic curves for (a) a single WTe 3D bundle (Figure 1d) and (b) a WTe thin film grown on a SiO_2/Si substrate measured at room temperature. The insets in (a) and (b) show an SEM image of the four-point probe measurement and an optical image of a device fabricated with a channel length of 20 μm, respectively. (c) Temperature dependence of the electrical resistance of the WTe network on a SiO_2/Si substrate under zero magnetic field ($B = 0$). Black and red curves represent the data taken on heating and cooling, as indicated by the arrows of corresponding color. The overlapping curves indicate reproducibility of the measurements. (d) Magnetoresistance as a function of B^2 for the corresponding sample in (c). Solid curves correspond to linear (40 to 80 K) and power law (10 to 30 K) fits.

voltage drop increases linearly with the current, following an ohmic relationship. With a nanowire length of 1.6 μm (inset Figure 4a) and an approximate cross-sectional area of 83 nm^2 (Figure 1d), the resistivity of the WTe bundle is estimated to be 1.3 $\mu\Omega$ m. This value is comparable to that of a single CNT bundle,[39,40] implying that the TMC nanowires exhibit excellent electrical conductivity. Additionally, the randomly oriented WTe thin film grown on a SiO_2/Si substrate exhibits a similar linear $I-V$ curve, and its sheet resistance is estimated to be 1.8 kΩ/sq (Figure 4b). Such low sheet resistance is likely due to the relatively low interbundle contact resistance, suggesting the potential application of WTe nanowires as transparent, flexible, and conductive films. The metallic behavior of the WTe network is confirmed by the temperature dependence of the electrical resistance. In Figure 4c, a monotonic decrease in resistance is observed as the temperature decreases from 300 to 10 K. The increase in resistance below 10 K is likely due to the electron localization effect in low-dimensional systems.[40] The data are reproducible, as evidenced by the overlapping heating and cooling curves. In addition, measurements taken on other samples, depicted in Figure S10, yielded similar results. Figure 4d shows the magnetoresistance (MR) of these conductive WTe networks plotted as a function of B^2 at various temperatures. Here, MR is defined as $[\rho(B) - \rho(0)]/\rho(0)$, where $\rho(0)$ and $\rho(B)$ refer to the resistivity in a zero and an applied magnetic field B, respectively. The MR increases with increasing magnetic field. The linear dependence of MR with B^2 observed from 80 to 40 K indicates classical metallic behavior subject to Lorentz forces.[41] In contrast, a nonlinear B^2 dependence is observed below 30 K. Such change in the field dependence can also be clearly seen for the $MR-B$ curves given in Figure S11. Considering the electrical resistance curve in Figure 4c, the cusp-like positive MR that appears at low temperature (<30 K) can be attributed to the weak antilocalization effect originating from the spin−orbit interaction, which usually predominates as material thickness decreases.[41] These findings demonstrate that TMC nanowires, having uniform crystal structure with varying aggregate forms, provide an ideal system to study 1D optical, electrical, and magnetic responses.

To confirm the transport results obtained, energy band structures of an isolated WTe nanowire, the 2D mono/bilayer sheet, and the 3D bundle (Figure S12) were also calculated based on the density functional theory (DFT). The corresponding band structures are displayed in Figure 5a−d and Figure S13. The results indicate that the isolated WTe nanowire is a narrow-gap semiconductor with an indirect gap of 18 meV (Figure 5a and Figure S13a). Its 2D and 3D counterparts, on the contrary, become metals. These changes can be understood from the wave functions near the Fermi level of the isolated and 2D WTe structures. As illustrated in Figure 5e, the conduction band minimum (CBM) at Γ point in Figure 5a mainly comes from the 5p orbitals of Te atoms, whereas the combined attribution from W (5d) and Te (5p) orbitals accounts for its valence band maximum (VBM). In the 2D (or 3D) assemblies, these wave functions eventually overlap with those of neighboring wires (Figure 5f), which hence leads to the increases of band widths. This changes the semiconducting nature of the WTe nanowire to a metallic one. The metallic band structure of the 3D assembly is consistent to the metallic transport properties observed in Figure 4 for the network of 3D bundles.

Finally, we discuss the effect of the substrate on the growth of TMC nanowires and corresponding mechanisms. Previous studies have reported that alkali metal halide aids the formation of highly volatile oxyhalide species and/or alkali metal complexes that promote TMDC growth.[29−32] Recently, the alkali metal was accountable to play a crucial role for initializing growth via a vapor−liquid−solid (VLS) mechanism.[31,32] The fact that the WTe nanowires are also grown by direct reaction of Te with $Na_2WO_4{\cdot}2H_2O$ (Figure S14) in the present study has hinted that a similar growth mechanism is involved. In this scenario, solid precursors first vaporize and

https://dx.doi.org/10.1021/acs.nanolett.0c03456
Nano Lett. 2021, 21, 243−249

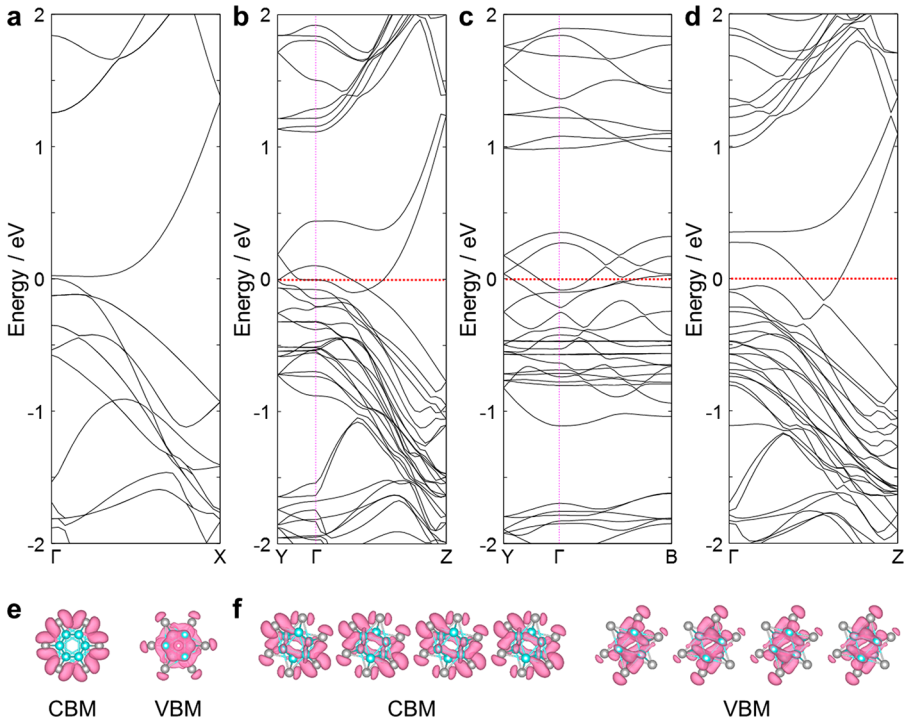

Figure 5. Electronic band structures. DFT-calculated band structures of (a) an isolated single WTe nanowire, (b) its 2D monolayer, and the 3D bundle along (c) Y−Γ−*B* line and (d) Γ−*Z* line, respectively. Fermi level is set to zero as a reference for (b−d). An isolated WTe nanowire is a narrow-gap semiconductor with an indirect gap of 18 meV (an enlarged image is shown in Figure S13a), whereas its collected 2D and 3D assemblies are metals. Squared wave functions of the CBM and VBM at Γ point with energies of (e) 0.02 and 0 eV in (a) and of (f) 0.1 and 0 eV in (b), respectively.

deposit onto the substrate surface, forming islands of molten intermediate droplets. When these droplets become supersaturated, the WTe nanowires start to emerge and elongate as the reaction proceeds. A root-growth model predominates over tip-growth as indicated by the radially extended wires with a shared nucleation center, as observed in Figure S15. With respect to the effect of the substrate, a close relationship between the mode of WTe nanowire growth and the supporting substrate is observed (Figure S16). Randomly oriented networks of TMC nanowires are usually formed on amorphous surfaces, such as the oxide (SiO_2) surface of Si wafers and quartz glass. In contrast, a single-crystal alumina (sapphire) substrate offers better control over the growth direction. The orientation of the nanowires varies depending on the crystal surface plane. For example, unidirectionally aligned nanowires are observed on the *a*- and *r*-planes of sapphire, while WTe nanowires on the *c*-plane grow in three different directions at 120° angles to one another (Figure 2c and Figure S16). Such directed growth may take place due to the gas flow, atomic step, faceted nanogrooves, or crystallographic-induced alignment.[42−45] Nonetheless, the influence of gas flow is unlikely as it fails to explain the different projections on the *c*-plane sapphire substrate. Besides, the cross-section images in Figure 1b, c indicate wire formation on a flat surface with no step edge nor grooves. The alignment is therefore attributable to the lattice-oriented anisotropic wire-substrate interaction, which has also been reported in the directed growth of carbon nanotubes[42,43] and nanowires such as GaN and ZnS.[44,45] As shown earlier in Figure 1b−d, the formation of nanowire-based 2D sheets and 3D bundles is also affected by the substrate. According to these results, the tendency to attain either the sheet or bundle configuration is determined by whether the wire−substrate interaction or the wire−wire interaction is dominant, respectively. The bundle formation could be also facilitated through the aggregation of molten intermediate droplets on the SiO_2 surface, which has larger surface roughness and different affinity compared to the Al_2O_3 surface.[32] These phenomena offer an opportunity for simultaneous control of the structural morphology, size, and geometric orientation of TMC nanowires as 1D vdW building blocks, benefiting the future design of nanowire-based materials for optimal properties.

CONCLUSIONS

In conclusion, the ability to achieve large-scale synthesis and manipulate the nanowire growth direction is important, as it provides a possible means for scalable, direct orientation patterning of TMC nanowires via surface engineering. The present findings offer a new platform for novel studies and applications of 1D vdW nanowire systems, contributing not only to new discoveries in basic low-dimension physics but also to the design of future applications in electronics and energy storage/conversion devices.

ASSOCIATED CONTENT

Supporting Information

The Supporting Information is available free of charge at https://pubs.acs.org/doi/10.1021/acs.nanolett.0c03456.

Experimental methods and supporting data for structural uniformity and crystallinity of suspended WTe bundles with the corresponding EDS measurements, decomposed WTe residue, surface morphology of the WTe network on SiO_2/Si and *a*-plane sapphire, coverage and crystal uniformity of the WTe network, topographic

https://dx.doi.org/10.1021/acs.nanolett.0c03456
Nano Lett. 2021, 21, 243−249

analysis of WTe nanowires, SEM of MoTe nanowires, polarized Raman characterization and optical absorption of WTe nanowires, transport measurements for different WTe devices, structural models for DFT calculations, electronic band structure of bilayer 2D WTe, tellurization of $Na_2WO_4 \cdot 2H_2O$, nucleation of WTe nanowires, and WTe growth on various surfaces (PDF)

AUTHOR INFORMATION

Corresponding Authors

Hong En Lim − *Department of Physics, Tokyo Metropolitan University, Hachioji 192-0397, Japan;* orcid.org/0000-0003-0347-8897; Email: lim@tmu.ac.jp

Yasumitsu Miyata − *Department of Physics, Tokyo Metropolitan University, Hachioji 192-0397, Japan;* orcid.org/0000-0002-9733-5119; Email: ymiyata@tmu.ac.jp

Authors

Yusuke Nakanishi − *Department of Physics, Tokyo Metropolitan University, Hachioji 192-0397, Japan;* orcid.org/0000-0001-8782-9556

Zheng Liu − *Innovative Functional Materials Research Institute, National Institute of Advanced Industrial Science and Technology (AIST), Nagoya 463-8560, Japan;* orcid.org/0000-0001-9095-7647

Jiang Pu − *Department of Applied Physics, Nagoya University, Nagoya 464-8603, Japan;* orcid.org/0000-0002-1676-2072

Mina Maruyama − *Department of Physics, Graduate School of Pure and Applied Sciences, University of Tsukuba, Tsukuba 305-8571, Japan;* orcid.org/0000-0002-2872-5543

Takahiko Endo − *Department of Physics, Tokyo Metropolitan University, Hachioji 192-0397, Japan*

Chisato Ando − *Department of Physics, Tokyo Metropolitan University, Hachioji 192-0397, Japan*

Hiroshi Shimizu − *Department of Physics, Tokyo Metropolitan University, Hachioji 192-0397, Japan*

Kazuhiro Yanagi − *Department of Physics, Tokyo Metropolitan University, Hachioji 192-0397, Japan;* orcid.org/0000-0002-7609-1493

Susumu Okada − *Department of Physics, Graduate School of Pure and Applied Sciences, University of Tsukuba, Tsukuba 305-8571, Japan*

Taishi Takenobu − *Department of Applied Physics, Nagoya University, Nagoya 464-8603, Japan*

Complete contact information is available at: https://pubs.acs.org/10.1021/acs.nanolett.0c03456

Author Contributions

H.E.L., Y.N., and Y.M. conceived the experiments. H.E.L., T.E., and C.A. conducted material growth. H.E.L., C.A., and Y.M. performed Raman, SEM, and AFM characterization. Z.L. carried out the STEM observations. Y.M. and K.Y. measured the optical absorption. C.A., H.S., Y.N., Y.M., and J.P. fabricated the devices and conducted electrical measurements. T.T. provided technical support and assisted data analyses of electrical measurements. M.M. and S.O. performed DFT calculations. H.E.L. and Y.M. wrote the paper. All authors discussed and commented on the manuscript.

Notes

The authors declare no competing financial interest.

ACKNOWLEDGMENTS

This work was supported by JST CREST (JPMJCR16F3), Grants-in-Aid for Scientific Research (B) (JP18H01832 and JP19H02543), and a Grant-in-Aid for Young Scientists (JP19K15393) from the Japan Society for the Promotion of Science (JSPS). Y.N. acknowledges support from JSPS KAKENHI (20H02572), Murata Science Foundation 2019 (H31-068), JKA 2020 (2020M-121), and its promotion funds from KEIRIN RACE. J.P. acknowledges support from JSPS KAKENHI (JP19K15383 and 20H05189). K.Y. acknowledges support by JSPS KAKENHI through Grant Number JP20H02573 and by JST CREST through Grant Number JPMJCR17I5. T.T. acknowledges support from JSPS KAKENHI (JP26102012, JP25000003, 19K22127, and JP17H01069) and JST CREST (JPMJCR17I5). This work was partially conducted at the AIST Nano-Processing Facility supported by "Nanotechnology Platform Program" of the Ministry of Education, Culture, Sports, Science and Technology (MEXT), Japan. Grant Number JPMXP09F19008709 and 20009034.

REFERENCES

(1) Kroto, H. W.; Heath, J. R.; O'Brien, S. C.; Curl, R. F.; Smalley, R. E. C_{60}: Buckminsterfullerene. *Nature* **1985**, *318* (6042), 162−163.

(2) Iijima, S.; Ichihashi, T. Single-Shell Carbon Nanotubes of 1-nm Diameter. *Nature* **1993**, *363* (6430), 603−605.

(3) Novoselov, K. S.; Geim, A. K.; Morozov, S. V.; Jiang, D.; Zhang, Y.; Dubonos, S. V.; Grigorieva, I. V.; Firsov, A. A. Electric Field Effect in Atomically Thin Carbon Films. *Science* **2004**, *306* (5696), 666−669.

(4) Novoselov, K. S.; Jiang, D.; Schedin, F.; Booth, T. J.; Khotkevich, V. V.; Morozov, S. V.; Geim, A. K. Two-Dimensional Atomic Crystals. *Proc. Natl. Acad. Sci. U. S. A.* **2005**, *102* (30), 10451−10453.

(5) Potel, M.; Chevrel, R.; Sergent, M.; Armici, J. C.; Decroux, M.; Fischer, Ø. New Pseudo-One-Dimensional Metals: $M_2Mo_6Se_6$ (M = Na, In, K, TI), $M_2Mo_6S_6$ (M = K, Rb, Cs), $M_2Mo_6Te_6$ (M = In, TI). *J. Solid State Chem.* **1980**, *35* (2), 286−290.

(6) Tarascon, J. M.; Hull, G. W.; DiSalvo, F. J. Facile Synthesis of Pseudo One-Monodimensional Ternary Molybdenum Chalcogenides $M_2Mo_6X_6$ (X = Se, Te; M = Li, Na. Cs). *Mater. Res. Bull.* **1984**, *19* (7), 915−924.

(7) Tarascon, J. M. Mo_6Se_6: A New Solid-State Electrode for Secondary Lithium Batteries. *J. Electrochem. Soc.* **1985**, *132* (9), 2089.

(8) Venkataraman, L.; Lieber, C. M. Molybdenum Selenide Molecular Wires as One-Dimensional Conductors. *Phys. Rev. Lett.* **1999**, *83* (25), 5334−5337.

(9) Venkataraman, L.; Hong, Y. S.; Kim, P. Electron Transport in a Multichannel One-Dimensional Conductor: Molybdenum Selenide Nanowires. *Phys. Rev. Lett.* **2006**, *96* (7), 076601.

(10) Xia, Y.; Wang, B.; Zhang, J.; Jin, Y.; Tian, H.; Ho, W.; Xu, H.; Jin, C.; Xie, M. Quantum Confined Tomonaga−Luttinger Liquid in Mo_6Se_6 Nanowires Converted from an Epitaxial $MoSe_2$ Monolayer. *Nano Lett.* **2020**, *20* (3), 2094−2099.

(11) Cheng, F.; Xu, H.; Xu, W.; Zhou, P.; Martin, J.; Loh, K. P. Controlled Growth of 1D $MoSe_2$ Nanoribbons with Spatially Modulated Edge States. *Nano Lett.* **2017**, *17* (2), 1116−1120.

(12) Poh, S. M.; Tan, S. J. R.; Zhao, X.; Chen, Z.; Abdelwahab, I.; Fu, D.; Xu, H.; Bao, Y.; Zhou, W.; Loh, K. P. Large Area Synthesis of 1D-$MoSe_2$ Using Molecular Beam Epitaxy. *Adv. Mater.* **2017**, *29* (12), 1605641.

(13) Chowdhury, T.; Kim, J.; Sadler, E. C.; Li, C.; Lee, S. W.; Jo, K.; Xu, W.; Gracias, D. H.; Drichko, N. V.; Jariwala, D.; Brintlinger, T. H.; Mueller, T.; Park, H.-G.; Kempa, T. J. Substrate-Directed Synthesis of MoS_2 Nanocrystals with Tunable Dimensionality and Optical Properties. *Nat. Nanotechnol.* **2020**, *15* (1), 29−34.

(14) Lin, J.; Cretu, O.; Zhou, W.; Suenaga, K.; Prasai, D.; Bolotin, K. I.; Cuong, N. T.; Otani, M.; Okada, S.; Lupini, A. R.; Idrobo, J.-C.; Caudel, D.; Burger, A.; Ghimire, N. J.; Yan, J.; Mandrus, D. G.; Pennycook, S. J.; Pantelides, S. T. Flexible Metallic Nanowires with Self-Adaptive Contacts to Semiconducting Transition-Metal Dichalcogenide Monolayers. *Nat. Nanotechnol.* **2014**, *9* (6), 436−442.
(15) Zhu, H.; Wang, Q.; Zhang, C.; Addou, R.; Cho, K.; Wallace, R. M.; Kim, M. J. New Mo_6Te_6 Sub-Nanometer-Diameter Nanowire Phase from 2H-$MoTe_2$. *Adv. Mater.* **2017**, *29* (18), 1606264.
(16) Kibsgaard, J.; Tuxen, A.; Levisen, M.; Lægsgaard, E.; Gemming, S.; Seifert, G.; Lauritsen, J. V.; Besenbacher, F. Atomic-Scale Structure of Mo_6S_6 Nanowires. *Nano Lett.* **2008**, *8* (11), 3928−3931.
(17) Yu, Y.; Wang, G.; Tan, Y.; Wu, N.; Zhang, X.-A.; Qin, S. Phase-Controlled Growth of One-Dimensional Mo_6Te_6 Nanowires and Two-Dimensional $MoTe_2$ Ultrathin Films Heterostructures. *Nano Lett.* **2018**, *18* (2), 675−681.
(18) Nagata, M.; Shukla, S.; Nakanishi, Y.; Liu, Z.; Lin, Y.-C.; Shiga, T.; Nakamura, Y.; Koyama, T.; Kishida, H.; Inoue, T.; Kanda, N.; Ohno, S.; Sakagawa, Y.; Suenaga, K.; Shinohara, H. Isolation of Single-Wired Transition-Metal Monochalcogenides by Carbon Nanotubes. *Nano Lett.* **2019**, *19* (8), 4845−4851.
(19) Kanda, N.; Nakanishi, Y.; Liu, D.; Liu, Z.; Inoue, T.; Miyata, Y.; Tománek, D.; Shinohara, H. Efficient Growth and Characterization of One-Dimensional Transition Metal Tellurides inside Carbon Nanotubes. *Nanoscale* **2020**, *12*, 17185−17190.
(20) Cassell, A. M.; Raymakers, J. A.; Kong, J.; Dai, H. J. Large Scale CVD Synthesis of Single-Walled Carbon Nanotubes. *J. Phys. Chem. B* **1999**, *103* (31), 6484−6492.
(21) Hata, K.; Futaba, D. N.; Mizuno, K.; Namai, T.; Yumura, M.; Iijima, S. Water-Assisted Highly Efficient Synthesis of Impurity-Free Single-Walled Carbon Nanotubes. *Science* **2004**, *306* (5700), 1362−1364.
(22) Li, X. S.; Cai, W. W.; An, J. H.; Kim, S.; Nah, J.; Yang, D. X.; Piner, R.; Velamakanni, A.; Jung, I.; Tutuc, E.; Banerjee, S. K.; Colombo, L.; Ruoff, R. S. Large-Area Synthesis of High-Quality and Uniform Graphene Films on Copper Foils. *Science* **2009**, *324* (5932), 1312−1314.
(23) Bae, S.; Kim, H.; Lee, Y.; Xu, X.; Park, J.-S.; Zheng, Y.; Balakrishnan, J.; Lei, T.; Ri Kim, H.; Song, Y. I.; Kim, Y.-J.; Kim, K. S.; Özyilmaz, B.; Ahn, J.-H.; Hong, B. H.; Iijima, S. Roll-to-Roll Production of 30-Inch Graphene Films for Transparent Electrodes. *Nat. Nanotechnol.* **2010**, *5* (8), 574−578.
(24) Suzuki, H.; Kaneko, T.; Shibuta, Y.; Ohno, M.; Maekawa, Y.; Kato, T. Wafer-Scale Fabrication and Growth Dynamics of Suspended Graphene Nanoribbon Arrays. *Nat. Commun.* **2016**, *7* (1), 11797.
(25) Lee, Y.-H.; Zhang, X.-Q.; Zhang, W.; Chang, M.-T.; Lin, C.-T.; Chang, K.-D.; Yu, Y.-C.; Wang, J. T.-W.; Chang, C.-S.; Li, L.-J.; Lin, T.-W. Synthesis of Large-Area MoS_2 Atomic Layers with Chemical Vapor Deposition. *Adv. Mater.* **2012**, *24* (17), 2320−2325.
(26) Liu, K.-K.; Zhang, W.; Lee, Y.-H.; Lin, Y.-C.; Chang, M.-T.; Su, C.-Y.; Chang, C.-S.; Li, H.; Shi, Y.; Zhang, H.; Lai, C.-S.; Li, L.-J. Growth of Large-Area and Highly Crystalline MoS_2 Thin Layers on Insulating Substrates. *Nano Lett.* **2012**, *12* (3), 1538−1544.
(27) Zhan, Y.; Liu, Z.; Najmaei, S.; Ajayan, P. M.; Lou, J. Large-Area Vapor-Phase Growth and Characterization of MoS_2 Atomic Layers on a SiO_2 Substrate. *Small* **2012**, *8* (7), 966−971.
(28) Kang, K.; Xie, S.; Huang, L.; Han, Y.; Huang, P. Y.; Mak, K. F.; Kim, C.-J.; Muller, D.; Park, J. High-Mobility Three-Atom-Thick Semiconducting Films with Wafer-Scale Homogeneity. *Nature* **2015**, *520* (7549), 656−660.
(29) Li, S.; Wang, S.; Tang, D.-M.; Zhao, W.; Xu, H.; Chu, L.; Bando, Y.; Golberg, D.; Eda, G. Halide-Assisted Atmospheric Pressure Growth of Large WSe_2 and WS_2 Monolayer Crystals. *Appl. Mater. Today* **2015**, *1* (1), 60−66.
(30) Zhou, J.; Lin, J.; Huang, X.; Zhou, Y.; Chen, Y.; Xia, J.; Wang, H.; Xie, Y.; Yu, H.; Lei, J.; Wu, D.; Liu, F.; Fu, Q.; Zeng, Q.; Hsu, C.-H.; Yang, C.; Lu, L.; Yu, T.; Shen, Z.; Lin, H.; Yakobson, B. I.; Liu, Q.; Suenaga, K.; Liu, G.; Liu, Z. A Library of Atomically Thin Metal Chalcogenides. *Nature* **2018**, *556* (7701), 355−359.
(31) Li, S.; Lin, Y.-C.; Zhao, W.; Wu, J.; Wang, Z.; Hu, Z.; Shen, Y.; Tang, D.-M.; Wang, J.; Zhang, Q.; Zhu, H.; Chu, L.; Zhao, W.; Liu, C.; Sun, Z.; Taniguchi, T.; Osada, M.; Chen, W.; Xu, Q.-H.; Wee, A. T. S.; Suenaga, K.; Ding, F.; Eda, G. Vapour−Liquid−Solid Growth of Monolayer MoS_2 Nanoribbons. *Nat. Mater.* **2018**, *17* (6), 535−542.
(32) Li, S.; Lin, Y.-C.; Liu, X.-Y.; Hu, Z.; Wu, J.; Nakajima, H.; Liu, S.; Okazaki, T.; Chen, W.; Minari, T.; Sakuma, Y.; Tsukagoshi, K.; Suenaga, K.; Taniguchi, T.; Osada, M. Wafer-Scale and Deterministic Patterned Growth of Monolayer MoS_2 via Vapor−Liquid−Solid Method. *Nanoscale* **2019**, *11* (34), 16122−16129.
(33) Duesberg, G. S.; Loa, I.; Burghard, M.; Syassen, K.; Roth, S. Polarized Raman Spectroscopy on Isolated Single-Wall Carbon Nanotubes. *Phys. Rev. Lett.* **2000**, *85* (25), 5436−5439.
(34) Jorio, A.; Souza Filho, A. G.; Dresselhaus, G.; Dresselhaus, M. S.; Swan, A. K.; Ünlü, M. S.; Goldberg, B. B.; Pimenta, M. A.; Hafner, J. H.; Lieber, C. M.; Saito, R. G-Band Resonant Raman Study of 62 Isolated Single-Wall Carbon Nanotubes. *Phys. Rev. B: Condens. Matter Mater. Phys.* **2002**, *65* (15), 155412.
(35) Xie, L.; Wang, H.; Jin, C.; Wang, X.; Jiao, L.; Suenaga, K.; Dai, H. Graphene Nanoribbons from Unzipped Carbon Nanotubes: Atomic Structures, Raman Spectroscopy, and Electrical Properties. *J. Am. Chem. Soc.* **2011**, *133* (27), 10394−10397.
(36) Xiong, Q.; Chen, G.; Gutierrez, H. R.; Eklund, P. C. Raman Scattering Studies of Individual Polar Semiconducting Nanowires: Phonon Splitting and Antenna Effects. *Appl. Phys. A: Mater. Sci. Process.* **2006**, *85* (3), 299−305.
(37) Möller, M.; de Lima, M. M.; Cantarero, A.; Dacal, L. C. O.; Madureira, J. R.; Iikawa, F.; Chiaramonte, T.; Cotta, M. A. Polarized and Resonant Raman Spectroscopy on Single InAs Nanowires. *Phys. Rev. B: Condens. Matter Mater. Phys.* **2011**, *84* (8), 085318.
(38) Wu, J.-B.; Zhao, H.; Li, Y.; Ohlberg, D.; Shi, W.; Wu, W.; Wang, H.; Tan, P.-H. Monolayer Molybdenum Disulfide Nanoribbons with High Optical Anisotropy. *Adv. Opt. Mater.* **2016**, *4* (5), 756−762.
(39) Thess, A.; Lee, R.; Nikolaev, P.; Dai, H.; Petit, P.; Robert, J.; Xu, C.; Lee, Y. H.; Kim, S. G.; Rinzler, A. G.; Colbert, D. T.; Scuseria, G. E.; Tománek, D.; Fischer, J. E.; Smalley, R. E. Crystalline Ropes of Metallic Carbon Nanotubes. *Science* **1996**, *273* (5274), 483−487.
(40) Fischer, J. E.; Dai, H.; Thess, A.; Lee, R.; Hanjani, N. M.; Dehaas, D. L.; Smalley, R. E. Metallic Resistivity in Crystalline Ropes of Single-Wall Carbon Nanotubes. *Phys. Rev. B: Condens. Matter Mater. Phys.* **1997**, *55* (8), R4921−R4924.
(41) Wang, L.; Gutiérrez-Lezama, I.; Barreteau, C.; Ubrig, N.; Giannini, E.; Morpurgo, A. F. Tuning Magnetotransport in a Compensated Semimetal at the Atomic Scale. *Nat. Commun.* **2015**, *6* (1), 8892.
(42) Ago, H.; Nakamura, K.; Ikeda, K.-I.; Uehara, N.; Ishigami, N.; Tsuji, M. Aligned Growth of Isolated Single-Walled Carbon Nanotubes Programmed by Atomic Arrangement of Substrate Surface. *Chem. Phys. Lett.* **2005**, *408* (4), 433−438.
(43) Han, S.; Liu, X.; Zhou, C. Template-Free Directional Growth of Single-Walled Carbon Nanotubes on a- and r-Plane Sapphire. *J. Am. Chem. Soc.* **2005**, *127* (15), 5294−5295.
(44) Tsivion, D.; Schvartzman, M.; Popovitz-Biro, R.; von Huth, P.; Joselevich, E. Guided Growth of Millimeter-Long Horizontal Nanowires with Controlled Orientations. *Science* **2011**, *333* (6045), 1003−1007.
(45) Rothman, A.; Forsht, T.; Danieli, Y.; Popovitz-Biro, R.; Rechav, K.; Houben, L.; Joselevich, E. Guided Growth of Horizontal ZnS Nanowires on Flat and Faceted Sapphire Surfaces. *J. Phys. Chem. C* **2018**, *122* (23), 12413−12420.

https://dx.doi.org/10.1021/acs.nanolett.0c03456
Nano Lett. 2021, 21, 243−249